Intrinsic and substrate induced spin-orbit interaction in chirally stacked trilayer graphene

Andor Kormányos[*] and Guido Burkard

Department of Physics, University of Konstanz, D-78464 Konstanz, Germany
(Received 26 October 2012; published 18 January 2013)

We present a combined group-theoretical and tight-binding approach to calculate the intrinsic spin-orbit coupling (SOC) in ABC stacked trilayer graphene. We find that compared to monolayer graphene (S. Konschuh, M. Gmitra, and J. Fabian [Phys. Rev. B **82**, 245412 (2010)]), a larger set of d orbitals (in particular the d_{z^2} orbital) needs to be taken into account. We also consider the intrinsic SOC in bilayer graphene, because the comparison between our tight-binding bilayer results and the density functional computations of S. Konschuh, M. Gmitra, D. Kochan, and J. Fabian [Phys. Rev. B **85**, 115423 (2012)] allows us to estimate the values of the trilayer SOC parameters as well. We also discuss the situation when a substrate or adatoms induce strong SOC in only one of the layers of bilayer or ABC trilayer graphene. Both for the case of intrinsic and externally induced SOC we derive effective Hamiltonians which describe the low-energy spin-orbit physics. We find that at the K point of the Brillouin zone the effect of Bychkov-Rashba type SOC is suppressed in bilayer and ABC trilayer graphene compared to monolayer graphene.

I. INTRODUCTION

The low-energy properties of multilayer graphene[1] depend crucially on the stacking order of the constituent graphene layers.[2–17] In the case of trilayer graphene, there are two stable stacking orders: (i) ABA or Bernard stacking and (ii) ABC or chiral stacking. Recent advances in sample fabrication methods have resulted in high-quality trilayer samples which can be used to probe many of the theoretical predictions.[12–18] ABC stacked trilayer graphene appears to be particularly exciting because it is expected to host a wealth of interesting phenomena, such as chiral quasiparticles with Berry phase 3π,[8] a Lifshitz transition of electronic bands due to trigonal warping,[8,11] band-gap opening in an external electric field,[2,4,5,8,10,11,14,18–20] and broken-symmetry phases at low electron densities,[21–24] to name a few.

Although there are a number of theoretical[2–11,19,20,27,28] and experimental[12–17,25–27] studies on the electronic properties of ABA and ABC stacked trilayer graphene, the spin-orbit coupling (SOC) in these systems has received much less attention. ABA trilayer graphene was considered in Ref. 29 within a framework of an effective low-energy theory, whereas the case ABC stacking was only briefly mentioned in Ref. 30. The understanding of spin-orbit interaction would be important to study other interesting and experimentally relevant phenomena such as spin relaxation,[31–34] weak localization,[32] or even spin Hall effect[35] in trilayer graphene. The recent report of Ref. 18 on the fabrication of high-mobility double-gated ABC trilayer graphene may open very promising new avenues for trilayer graphene spintronics as well, similarly to the monolayer case where highly efficient spin transport has recently been reported,[36] but with the additional advantage that external gates can open a band gap in ABC trilayer graphene.

In this paper we aim to make the first steps towards a detailed understanding of the SOC in chirally stacked trilayer graphene. We start by investigating the case when the system has inversion symmetry, i.e., in the absence of external electric fields, adatoms, or a substrate. This is the case of *intrinsic* SOC. The intrinsic SOC opens a band gap at the band-degeneracy points without introducing spin polarization. Previous *ab*

initio calculations on monolayer[37,38] and bilayer[40] graphene provided strong evidence that the key to the understanding the SOC in *flat* graphene systems is to take into account the (nominally unoccupied) d orbitals in the description of electronic bands. Here we take the same view and by generalizing the work of Ref. 39 derive the intrinsic SOC Hamiltonian for ABC trilayer graphene. It turns out that the most important d orbitals to take into account are the d_{xz}, d_{yz}, and d_{z^2} orbitals. While the former two have been considered in Ref. 39 in the context of monolayer graphene, the latter one is important to understand the SOC in AB and ABC graphene. We obtain explicit expressions for the SOC constants in terms of Slater-Koster[41] hopping parameters. We also rederive the intrinsic SO Hamiltonian for bilayer graphene.[30,40] Through the comparison of our trilayer and bilayer analytical results with the recent *ab initio* calculations of Ref. 40 we are able to make predictions for the actual values of the SOC parameters in ABC trilayer graphene. The theory involves electronic bands which are far from the Fermi energy E_F but are coupled to the physically important low-energy bands close to E_F and hence complicate the description of the electronic properties. Therefore, we derive an effective low-energy Hamiltonian and calculate its spectrum. This helps us to understand how SOC lifts certain degeneracies of the electronic bands.

Generally speaking, due to the low atomic number of carbon, the intrinsic SOC in single and multilayer graphene is weak (according to our prediction, the SOC parameters are of the order of 10 μeV in ABC trilayer, the same as in monolayer[37–39,44] and bilayer[40] graphene). Recently however, there have been exciting theoretical proposals to enhance the strength of SOC in monolayer graphene and hence, e.g., make the quantum spin Hall state[35] observable. These proposals suggest deposition of indium or thallium atoms[53] or to bring graphene into proximity with topological insulators.[56] Indeed, very recently the combined experimental and theoretical work of Ref. 57 has provided evidence of a large (10–100 meV) spin-orbit gap in monolayer graphene on nickel substrate with intercalated gold atoms. Motivated by these studies we also discuss what might be a minimal model to describe the case
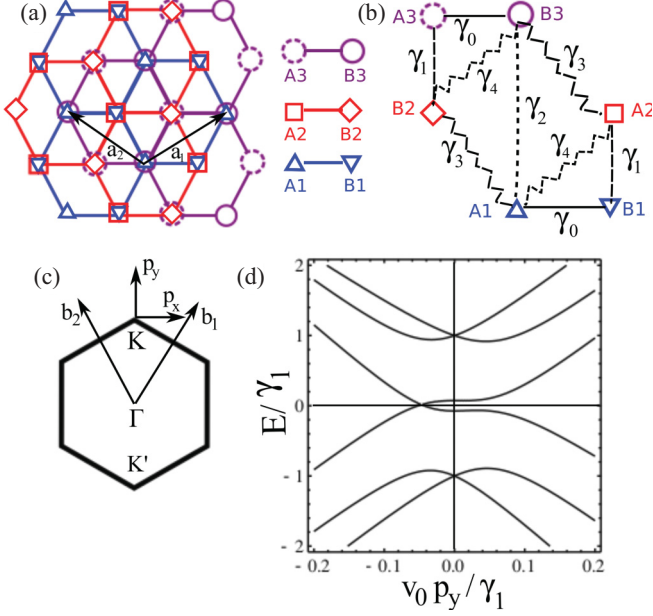
FIG. 1. (Color online) Lattice and band structure of ABC trilayer graphene. (a) Lattice structure, where atoms on different layers are indicated with different symbols. $\mathbf{a}_1$ and $\mathbf{a}_2$ are the two lattice vectors. (b) Schematic side view of the unit cell with the most important hopping amplitudes. (c) Schematic of the Brillouin zone with reciprocal lattice vectors $\mathbf{b}_1$, $\mathbf{b}_2$, the high-symmetry points Γ, K, and K', and the momentum $\mathbf{p} = (p_x, p_y)$ measured from K. (d) Schematic of the band structure at the K point of the Brillouin zone. The velocity v_0 is given by $v_0 = \sqrt{3}/2a\gamma_0/\hbar$, where a is the lattice constant: $a = |\mathbf{a}_1|$.

where the the SOC is strongly enhanced in only one of the layers of bilayer and ABC trilayer graphene.

Our work is organized as follows. In Sec. II we present the tight-binding (TB) model of ABC stacked graphene and introduce certain notations that we will be using in subsequent sections. In Sec. III, employing group-theoretical considerations and the Slater-Koster[41] (SK) parametrization of transfer integrals, we derive the SOC Hamiltonian in atomistic approximation at the K point of the Brillouin zone. We repeat this calculation for bilayer graphene in Sec. IV so that in Sec. V we can make predictions for the actual values of the SOC parameters. Next, in Sec. VI, using $\mathbf{k} \cdot \mathbf{p}$ theory and the Schrieffer-Wolff transformation,[46,47] we derive an effective low-energy SOC Hamiltonian which is valid for wave vectors around the K (K') point. Finally, in Sec. VII, we consider the case when SOC is enhanced in one of the graphene layers with respect to the other(s).

II. TIGHT-BINDING MODEL

The basic electronic properties of the ABC trilayer are well captured by the effective mass model which is derived assuming one p_z-type atomic orbital per carbon atom. This model has been discussed in detail in Refs. 8 and 11; therefore we give only a very short introduction here (see also Fig. 1).

There are six carbon atoms in the unit cell of ABC trilayer graphene, usually denoted by A1, B1, A2, B2, A3, B3, where A and B denote the sublattices and $j = 1,2,3$ is the layer

index. The parameters appearing in the effective model are γ_0 for the intralayer Aj-Bj nearest-neighbor hopping, γ_1 for the interlayer hopping between sites B1-A2 and B2-A3, γ_3 (γ_4) describes weaker nearest-layer hopping between atoms belonging to different (the same) sublattice, and finally γ_2 denotes the direct hopping between sites A1 and B3 that lie on the same vertical line in the outer layers 1 and 3. These hoppings can be obtained by, e.g., fitting the numerically calculated band structure with a TB model.[7,11] The six p_z orbitals in the unit cell give rise to six electronic bands.[8,11] As shown in Fig. 1(d), at the K (K') point of the Brillouin zone (BZ) two of these bands lie close to the Fermi energy $E_F = 0$ and we will refer to them as "low-energy" states. In addition, there are four "split-off" states far from E_F at energies $E = \pm\gamma_1$.

To obtain the intrinsic SOC Hamiltonian of ABC trilayer graphene we generalize the main idea of Ref. 39 where the SOC of monolayer graphene was discussed. Using group-theoretical considerations and density functional theory (DFT) calculations it was shown in Ref. 39 that in the case of monolayer graphene the main contribution to the intrinsic SOC comes from the admixture of p_z orbitals with some of the (nominally unoccupied) d orbitals, namely, with the d_{xz} and d_{yz} orbitals. The other d orbitals, d_{z^2}, d_{xy}, and $d_{x^2-y^2}$, play no role due to the fact that they are symmetric with respect to the mirror reflection $\sigma_h : (x,y,z) \rightarrow (x,y,-z)$ to the plane of the graphene layer, whereas p_z is antisymmetric. The importance of the d orbitals for the understanding of SOC in monolayer graphene was also pointed out in Ref. 38.

The symmetry group of ABC stacked trilayer graphene is $R\bar{3}m$ (D_{3d}) which does not contain the mirror reflection σ_h. Therefore, from a symmetry point of view, in an approach similar to Ref. 39, all d orbitals need to be taken into account. To derive a TB model one should therefore use as basis set the Bloch wave functions

$$\Psi_\beta^{\alpha j}(\mathbf{r},\mathbf{k}) = \frac{1}{\sqrt{N}} \sum_n e^{i\mathbf{k}\cdot(\mathbf{R}_n+\mathbf{t}_\alpha)} \Phi_\beta^j(\mathbf{r} - (\mathbf{R}_n + \mathbf{t}_\alpha)), \quad (1)$$

where the wave vector $\mathbf{k}$ is measured from the Γ point of the BZ (see Fig. 1), $\alpha j = \{$A1,A2,A3,B1,B2,B3$\}$ is a composite index for the sublattice $\alpha = \{$A, B$\}$ and layer $j = \{1,2,3\}$ indices, and Φ_β^j denotes the atomic orbitals of type $\beta = \{p_z, d_{z^2}, d_{xz}, d_{yz}, d_{xy}, d_{x^2-y^2}\}$ in layer j. The summation runs over all Bravais lattice vectors $\mathbf{R}_n$, whereas the vectors $\mathbf{t}_\alpha$ give the position of atom α in the two-dimensional unit cell. We use a coordinate system where the primitive lattice vectors are $\mathbf{a}_1 = \frac{a}{2}(\sqrt{3},1)$ and $\mathbf{a}_2 = \frac{a}{2}(-\sqrt{3},1)$, and the positions of the atoms in the unit cell are $\mathbf{t}_{A1} = \mathbf{t}_{B3} = (0,0)$, $\mathbf{t}_{A2} = \mathbf{t}_{B1} = \frac{a}{2}(-\frac{1}{\sqrt{3}},1)$, and $\mathbf{t}_{A3} = \mathbf{t}_{B2} = \frac{a}{2}(\frac{1}{\sqrt{3}},1)$, where $a = 2.46$ Å is the lattice constant. The K and K' points of the Brillouin zone, which are important for the low-energy physics discussed in this paper, can be found at $K = (0, \frac{4\pi}{3a})$, $K' = (0, -\frac{4\pi}{3a})$.

The symmetry group of the lattice contains threefold rotations by $\pm 2\pi/3$, about an axis perpendicular to the graphene layers. Since the atomic orbitals $d_{xz}, d_{yz}, d_{xy}, d_{x^2-y^2}$ themselves do not possess this symmetry, instead of $\Psi_\beta^{\alpha j}(\mathbf{r},\mathbf{k})$ given in Eq. (1) we will use Bloch states which depend on $\frac{1}{\sqrt{2}}(d_{xz} \pm id_{yz}) \sim \mp Y_2^{\pm 1}$, $\frac{1}{\sqrt{2}}(d_{x^2-y^2} \pm id_{xy}) \sim Y_2^{\pm 2}$ (rotating orbitals), where Y_l^m are spherical harmonics. Taking into

account that $p_z \sim Y_1^0$ and $d_{z^2} \sim Y_2^0$, the Bloch states we use as basis will be denoted by $\Psi_{l,m_l}^{\alpha j}(\mathbf{r},\mathbf{k})$, where $l = 1,2$ and $m_1 = 0$, whereas m_2 can take all allowed values $m_2 = -2 \ldots 2$. Often, we will need a linear combination of two of these basis functions where both of the basis functions have the same quantum number l but one of them is centered on an A-type atom and the other one is on a B-type atom, e.g., $\frac{1}{\sqrt{2}}[\Psi_{1,0}^{A1}(\mathbf{r},\mathbf{k}) - \Psi_{1,0}^{B3}(\mathbf{r},\mathbf{k})]$. As a shorthand notation, we will denote the symmetric combination of two such basis functions by $\Psi_{l,m,m'}^{j,j'}(\mathbf{r},\mathbf{k}) = \frac{1}{\sqrt{2}}[\Psi_{l,m}^{Aj}(\mathbf{r},\mathbf{k}) + \Psi_{l,m'}^{Bj'}(\mathbf{r},\mathbf{k})]$ and the antisymmetric one with $\overline{\Psi_{l,m,m'}^{j,j'}}(\mathbf{r},\mathbf{k}) = \frac{1}{\sqrt{2}}[\Psi_{l,m}^{Aj}(\mathbf{r},\mathbf{k}) - \Psi_{l,m'}^{Bj'}(\mathbf{r},\mathbf{k})]$. The first upper index j in $\Psi_{l,m,m'}^{j,j'}$ always denotes the layer index of the atomic orbital centered on the A-type atom, the second upper index j' is the layer index for the orbital centered on the B-type atom, the first lower index l is the common angular momentum quantum number, and finally, the second and the third lower indices m, m' give the magnetic quantum number in the same manner as the upper indices give the layer index. To lighten the notation, we will usually suppress the dependence of the Bloch functions on $(\mathbf{r},\mathbf{k})$ and use the bra-ket notation, e.g., $|\Psi_{1,0,0}^{1,3}\rangle$, $|\overline{\Psi_{1,0,0}^{1,3}}\rangle$.

The derivation of the spin-orbit Hamiltonian proceeds in the same spirit as in Ref. [39]: (i) First, we neglect the spin degree of freedom. Using the Slater-Koster parametrization to describe the hopping integrals $\langle \Psi_{l,m,m'}^{j,j'} | \hat{\mathcal{H}} | \Psi_{l',m'',m'''}^{j'',j'''} \rangle$ ($\hat{\mathcal{H}}$ is the single-particle Hamiltonian of the system) at a high symmetry point (the K point) of the Brillouin zone and group-theoretical considerations we obtain certain effective Bloch wave functions which comprise p_z and d atomic orbitals centered on different atoms; (ii) using these effective wave functions we calculate the matrix elements of the spin-orbit Hamiltonian in atomic approximation, and (iii) employing the $\mathbf{k} \cdot \mathbf{p}$ theory we obtain the bands around the K point and then we derive an effective low-energy Hamiltonian.

III. INTRINSIC SOC

If, in addition to the p_z orbitals, we include also the d orbitals into our basis, there will be six basis functions $|\Psi_{l,m}^{\alpha j}\rangle$ centered on each of the six carbon atoms in the unit cell and hence the TB Hamiltonian H_{ABC}, which is straightforward to calculate in the SK parametrization, a 36×36 matrix. By, e.g., numerically diagonalizing this matrix one would find that the p_z orbitals hybridize with some of the d orbitals and one could see how the low-energy and the split-off states, obtained in the first instance by neglecting the d orbitals, are modified. According to band theory each state at the K point should belong to one of the irreducible representations of the small group of the K point,[43] which is 32 (D_3) in this case. This group has two one-dimensional irreducible representation, denoted by Γ_{A_1} and Γ_{A_2}, respectively, and a two-dimensional one denoted by Γ_E (see Appendix A). The matrix elements of H_{ABC} between basis states corresponding to different irreducible representations of D_3 are zero.[43] In other words, H_{ABC} can be block diagonalized by choosing suitable linear combinations of the basis functions $|\Psi_{l,m}^{\alpha j}\rangle$ such that the new basis functions transform as the irreducible representations

of the group D_3 because the hybridization between p_z and d orbitals will preserve the symmetry properties. A group-theoretical analysis of the problem shows that in a suitable basis H_{ABC} is block diagonal having (i) two 6×6 blocks which we denote by $H_{\Gamma_{A_1}}$ and $H_{\Gamma_{A_2}}$, corresponding to basis states with Γ_{A_1} and Γ_{A_2} symmetry, and (ii) there is one 24×24 block H_{Γ_E} corresponding to states with Γ_E symmetry. (The basis vectors with Γ_{A_1}, Γ_{A_2}, and Γ_E symmetries are listed in Appendix A, Table VII.) As a concrete example we will consider $H_{\Gamma_{A_1}}$ and discuss how one can extract an effective orbital in which p_z atomic orbitals with large weight and d orbitals with small weight are admixed. The calculation for $H_{\Gamma_{A_2}}$ and H_{Γ_E} cases is analogous and will be presented only briefly.

The basis states transforming as the irreducible representation Γ_{A_1} are $|\overline{\Psi_{1,0,0}^{1,3}}\rangle$, $|\Psi_{2,1,-1}^{3,1}\rangle$, $|\Psi_{2,0,0}^{1,3}\rangle$, $|\Psi_{2,-2,2}^{3,1}\rangle$, $|\Psi_{2,-1,1}^{2,2}\rangle$, and $|\Psi_{2,2,-2}^{2,2}\rangle$. The TB Hamiltonian $H_{\Gamma_{A_1}}$ can be further divided into 3×3 blocks:

$$H_{\Gamma_{A_1}} = \begin{pmatrix} H_{pd}^{A_1} & W^{A_1} \\ (W^{A_1})^\dagger & H_{dd}^{A_1} \end{pmatrix}. \qquad (2)$$

Explicitly, the upper left block $H_{pd}^{A_1}$, corresponding to the basis states $|\overline{\Psi_{1,0,0}^{1,3}}\rangle$, $|\Psi_{2,1,-1}^{3,1}\rangle$, and $|\Psi_{2,0,0}^{1,3}\rangle$, reads

$$H_{pd}^{A_1} = \begin{pmatrix} \varepsilon_p - \gamma_2 & \frac{3}{\sqrt{2}} V_{pd\pi} & V_{pd\sigma}^{A1,B3} \\ \frac{3}{\sqrt{2}} V_{pd\pi} & \varepsilon_d & 0 \\ V_{pd\sigma}^{A1,B3} & 0 & \varepsilon_d + V_{dd\sigma}^{A1,B3} \end{pmatrix}, \qquad (3)$$

where the upper indices A1, B3 on the SK parameters indicate the atomic sites between which the hopping takes place. The parameter $V_{pd\pi}$ describes hopping between A- and B-type atoms within the same graphene layer and we assume that its value is the same in all three layers. The matrix elements in W^{A_1} of Hamiltonian (2) are either zero[48] or describe skew hoppings between the p_z and d orbitals located on different atoms. We assume that these skew hoppings are much smaller than both the vertical hopping $V_{pd\sigma}^{A1,B3}$ and $V_{pd\pi}$. This is not a crucial assumption and the neglected skew hoppings can be taken into account in a straightforward manner. However, it simplifies the lengthy algebra that follows and we believe it yields qualitatively correct results (see Sec. IV). With $W^{A_1} \approx 0$ we see that $H_{dd}^{A_1}$ (corresponding to the basis functions $|\Psi_{2,-2,2}^{3,1}\rangle$, $|\Psi_{2,-1,1}^{2,2}\rangle$, and $|\Psi_{2,2,-2}^{2,2}\rangle$) is decoupled from H_{pd} and that this latter matrix describes the hybridization between the p_z orbital based basis vector $|\overline{\Psi_{1,0,0}^{1,3}}\rangle$ and the basis vectors $|\Psi_{2,1,-1}^{3,1}\rangle$, $|\Psi_{2,0,0}^{1,3}\rangle$ involving d_{xz}, d_{yz}, and d_{z^2} orbitals. By diagonalizing $H_{pd}^{A_1}$ one could find out how the energy $\varepsilon_{A_1} = \varepsilon_p - \gamma_2$ of one of the low-energy states is modified by the d orbitals. The secular equation $\det(H_{pd}^{A_1} - \varepsilon I) = 0$ leads to a cubic equation in ε and the solutions can only be expressed using the Cardano formula. Instead, we next perform a Schrieffer-Wolff transformation (Löwdin partitioning) $\tilde{H}_{pd}^{A_1} = e^{-S} H_{pd}^{A_1} e^S$ to approximately block-diagonalize $H_{pd}^{A_1}$ into a 1×1 and a 2×2 block by eliminating the matrix elements between $|\overline{\Psi_{1,0,0}^{1,3}}\rangle$ on one hand and $|\Psi_{2,1,-1}^{3,1}\rangle$, $|\Psi_{2,0,0}^{1,3}\rangle$ on the other hand. (A detailed discussion

of this method can be found in, e.g., Refs. 46 and 47.) The matrix S is anti-Hermitian: $S^\dagger = -S$ and only its nondiagonal blocks S_{pd} and $-S_{pd}^\dagger$ are nonzero. In first order[46] of the coupling matrix elements $V_{pd\pi}$ and $V_{pd\sigma}^{A1,B3}$ one finds that

$$S_{pd}^{(1)} = -\left(\frac{\bar{V}_{pd\pi}}{\delta\varepsilon_{pd} - \gamma_2}, \frac{V_{pd\sigma}^{A1,B3}}{\delta\varepsilon_{pd} - \tilde{\gamma}_2} \right), \qquad (4)$$

where $\bar{V}_{pd\pi} = \frac{3}{\sqrt{2}} V_{pd\pi}$, $\delta\varepsilon_{pd} = \varepsilon_p - \varepsilon_d$, and $\tilde{\gamma}_2 = \gamma_2 + V_{dd\sigma}^{A1,B3}$. The 1×1 block of $\tilde{H}_{pd}^{A_1}$ reads $\tilde{\varepsilon}_{A_1} = \varepsilon_p - \gamma_2 + \bar{V}_{pd\pi}^2/(\delta\varepsilon_{pd} - \gamma_2) + (V_{pd\sigma}^{A1,B3})^2/(\delta\varepsilon_{pd} - \tilde{\gamma}_2)$; this means that the energy ε_{A_1} of the low-energy state is shifted by $\bar{V}_{pd\pi}^2/(\delta\varepsilon_{pd} - \gamma_2) + (V_{pd\sigma}^{A1,B3})^2/(\delta\varepsilon_{pd} - \tilde{\gamma}_2)$. While the Schrieffer-Wolff transformation is usually used to obtain effective Hamiltonians, one can also obtain the new basis in which $\tilde{H}_{pd}^{A_1}$ is block diagonal. Making the approximation $e^{-S} \approx 1 - S$ (see Ref. 49) we find that the purely p_z-like state $|\overline{\Psi_{1,0,0}^{1,3}}\rangle$ is transformed into

$$|\Psi_{\Gamma_{A_1}}^{p_z}\rangle = |\overline{\Psi_{1,0,0}^{1,3}}\rangle + \frac{\bar{V}_{pd\pi}}{\delta\varepsilon_{pd} - \gamma_2}|\Psi_{2,1,-1}^{3,1}\rangle + \frac{V_{pd\sigma}^{A1,B3}}{\delta\varepsilon_{pd} - \tilde{\gamma}_2}|\Psi_{2,0,0}^{1,3}\rangle; \qquad (5)$$

i.e., it is admixed with two other basis vectors containing d_{xz}, d_{yz}, and d_{z^2} orbitals. Since $|\Psi_{\Gamma_{A_1}}^{p_z}\rangle$ corresponds to a 1×1 and hence diagonal block of $\tilde{H}_{pd}$, it is an approximate eigenvector of $H_{pd}^{A_1}$ with energy $\tilde{\varepsilon}_{A_1}$. The upper index p_z in $|\Psi_{\Gamma_{A_1}}^{p_z}\rangle$ is meant to indicate that in this state p_z orbitals have the largest weight. There are two other states with Γ_{A_1} symmetry which could be obtained by diagonalizing the remaining 2×2 block of $\tilde{H}_{pd}^{A_1}$. In these states $|\Psi_{2,1,-1}^{3,1}\rangle$ and $|\Psi_{2,0,0}^{1,3}\rangle$ would have large weight. They are however far remote in energy from $|\Psi_{\Gamma_{A_1}}^{p_z}\rangle$ and therefore play no role in our further considerations. The situation will be similar in the case of the two other irreducible representations, Γ_{A_2} and Γ_E; therefore we will suppress the upper index p_z henceforth in the notation of the physically important approximate eigenstates.

We now briefly discuss the symmetry classes Γ_{A_2} and Γ_E. The calculation for the other 6×6 block of H_{ABC} with Γ_{A_2} symmetry is completely analogous to the Γ_{A_1} case; the resulting approximate eigenvector, $|\Psi_{\Gamma_{A_2}}\rangle$, is shown in the left column of Table IV. Its energy, apart from the shift due to the d orbitals, which will be neglected, is $\varepsilon_{A_2} = \varepsilon_p + \gamma_2$.

The matrix block corresponding to states with Γ_E symmetry can be written as

$$H_{\Gamma_E} = \begin{pmatrix} H_{pp}^E & W_{pd}^E \\ (W_{pd}^E)^\dagger & H_{dd}^E \end{pmatrix}. \qquad (6)$$

Here the 4×4 block H_{pp}^E contains the matrix elements between the basis vectors $|\Psi_{1,0,0}^{2,1}\rangle, |\Psi_{1,0,0}^{3,2}\rangle, |\overline{\Psi_{1,0,0}^{2,1}}\rangle, |\overline{\Psi_{1,0,0}^{3,2}}\rangle$; the 4×20 block W_{pd}^E is the coupling matrix between the above shown p_z orbital based basis vectors and the d orbitals based basis vectors. (The full set of basis vectors for each of the three symmetry classes is listed in Appendix A.) A direct calculation shows that H_{pp} is a diagonal matrix with $\varepsilon_p + \gamma_1, \varepsilon_p + \gamma_1, \varepsilon_p - \gamma_1, \varepsilon_p - \gamma_1$ entries. Earlier we have referred to these states

TABLE I. Intrinsic spin-orbit Hamiltonian τH_{so}^{ABC} in the symmetry basis. Here $\tau = +1$ (-1) corresponds to the K (K') point.

SOC	$\Psi_{\Gamma_{A_1}}$	$\Psi_{\Gamma_{A_2}}$	$\Psi_{\Gamma_{E_{1,1}}}$	$\Psi_{\Gamma_{E_{1,2}}}$	$\Psi_{\Gamma_{E_{2,1}}}$	$\Psi_{\Gamma_{E_{2,2}}}$
$\Psi_{\Gamma_{A_1}}$	0	$\lambda_{1/2}S_z^\tau$	$\lambda_{1/3}^{E_1}S_+^\tau$	$\lambda_{1/3}^{E_1}S_-^\tau$	$-\lambda_{1/3}^{E_2}S_+^\tau$	$\lambda_{1/3}^{E_2}S_-^\tau$
$\Psi_{\Gamma_{A_2}}$	$\lambda_{1/2}S_z$	0	$-\lambda_{2/3}^{E_1}S_+^\tau$	$\lambda_{2/3}^{E_1}S_-^\tau$	$\lambda_{2/3}^{E_2}S_+^\tau$	$\lambda_{2/3}^{E_2}S_-^\tau$
$\Psi_{\Gamma_{E_{1,1}}}$	$\lambda_{1/3}^{E_1}S_-^\tau$	$-\lambda_{2/3}^{E_1}S_-^\tau$	0	0	$\lambda_{3/3}^z S_z$	$\lambda_{3/3}S_+^\tau$
$\Psi_{\Gamma_{E_{1,2}}}$	$\lambda_{1/3}^{E_1}S_+^\tau$	$\lambda_{2/3}^{E_1}S_+^\tau$	0	0	$\lambda_{3/3}S_-^\tau$	$\lambda_{3/3}^z S_z$
$\Psi_{\Gamma_{E_{2,1}}}$	$-\lambda_{1/3}^{E_2}S_-^\tau$	$\lambda_{2/3}^{E_2}S_-^\tau$	$\lambda_{3/3}^z S_z$	$\lambda_{3/3}S_+^\tau$	0	0
$\Psi_{\Gamma_{E_{2,2}}}$	$\lambda_{1/3}^{E_2}S_+^\tau$	$\lambda_{2/3}^{E_2}S_+^\tau$	$\lambda_{3/3}S_-^\tau$	$\lambda_{3/3}^z S_z$	0	0

as "split-off" states. Since H_{pp}^E is diagonal, its approximate eigenvectors $|\Psi_{\Gamma_{E_{1,1}}}\rangle$, $|\Psi_{\Gamma_{E_{1,2}}}\rangle$, $|\Psi_{\Gamma_{E_{2,1}}}\rangle$, and $|\Psi_{\Gamma_{E_{2,2}}}\rangle$, which are listed in Table IV, can be obtained in exactly the same way as $|\Psi_{\Gamma_{A_1}}\rangle$.

We will refer to the basis formed from the physically important approximate eigenvectors $\{|\Psi_{\Gamma_{A_1}}\rangle, |\Psi_{\Gamma_{A_2}}\rangle, |\Psi_{\Gamma_{E_{1,1}}}\rangle, |\Psi_{\Gamma_{E_{1,2}}}\rangle, |\Psi_{\Gamma_{E_{2,1}}}\rangle, |\Psi_{\Gamma_{E_{2,2}}}\rangle\}$ as the "symmetry basis" henceforth. (The symmetry basis for the K' point can be obtained by complex-conjugation.) Looking at these basis vectors we see that in contrast to monolayer graphene,[39] where only d_{xz} and d_{yz} orbitals hybridize with the p_z orbital, here also the d_{z^2} orbitals are admixed. As will be shown below, the admixture of d_{z^2} orbitals is crucial to obtain the nondiagonal elements of the SOC Hamiltonian.

We can now proceed to calculate the SOC Hamiltonian. This can be done in the atomic approximation, whereby the spin-orbit interaction is described by the Hamiltonian

$$\hat{H}_{SO}^{\text{atomic}} = \frac{\hbar}{4m_e^2 c^2} \frac{1}{r} \frac{dV(r)}{dr} \mathbf{L} \cdot \mathbf{S}. \qquad (7)$$

Here $V(r)$ is the spherically symmetric atomic potential, $\mathbf{L}$ is the angular momentum operator, and $\mathbf{S} = (S_x, S_y)$ is a vector of spin Pauli matrices S_x, S_y (with eigenvalues ± 1). Introducing the spinful symmetry basis functions by $|\Psi_\mu\rangle \rightarrow |\Psi_\mu \otimes s\rangle$, where $s = \{\uparrow, \downarrow\}$ denotes the spin degree of freedom and noting that $\mathbf{L} \cdot \mathbf{S} = L_z S_z + L_+ S_- + L_- S_+$, where $L_\pm = L_x \pm iL_y$ and $S_\pm = \frac{1}{2}(S_x \pm iS_y)$, it is straightforward to calculate the matrix elements $(H_{so}^{ABC})_{\mu,\nu} = \langle\Psi_\mu|\hat{H}_{SO}^{\text{atomic}}|\Psi_\nu\rangle$ in the symmetry basis introduced earlier. Using the notation $S_\pm^\tau = \frac{1}{2}(S_x \pm i\tau \cdot S_y)$, where $\tau = +1$ (-1) corresponds to the K (K') point of the BZ, the result is shown in Table I.

The SOC Hamiltonian shown in Table I is the main result of this section. Explicit expressions in terms of SK parameters for the coupling constants appearing in Table I can be found in Table IV. In contrast to previous works where SOC in ABC trilayer was discussed,[30,45] we find that the number of SOC parameters is seven.[50] As we will show, $\lambda_{1/3}^{E_1}, \lambda_{1/3}^{E_2}, \lambda_{2/3}^{E_1}$, and $\lambda_{2/3}^{E_2}$ are related to interlayer SOC and calculations which are based on the symmetry properties of low-energy effective Hamiltonians may not capture them. The $\lambda_{3/3}$ parameter ensures that the otherwise fourfold degeneracy of the split-off states at the K point is lifted, as it is dictated by general group-theoretical considerations.[42,43] These five parameters are proportional to the product $V_{pd\pi} V_{pd\sigma}$ and they could not be obtained considering only the d_{xz}, d_{yz} orbitals and in-plane

TABLE II. τH_{so}^{ABC} in the basis of effective p_z orbitals.

SOC	Ψ_{eff}^{A1}	Ψ_{eff}^{B3}	Ψ_{eff}^{B1}	Ψ_{eff}^{A2}	Ψ_{eff}^{B2}	Ψ_{eff}^{A3}
Ψ_{eff}^{A1}	$\lambda_{1/2}\, S_z$	0	$\lambda_2\, S_+^\tau$	$\lambda_1\, S_+^\tau$	$\lambda_4\, S_-^\tau$	$\lambda_3\, S_-^\tau$
Ψ_{eff}^{B3}	0	$-\lambda_{1/2}\, S_z$	$-\lambda_3\, S_+^\tau$	$-\lambda_4\, S_+^\tau$	$-\lambda_1\, S_-^\tau$	$-\lambda_2\, S_-^\tau$
Ψ_{eff}^{B1}	$\lambda_2\, S_-^\tau$	$-\lambda_3\, S_-^\tau$	$-\lambda_{3/3}^z\, S_z$	0	$-\lambda_{3/3}\, S_+^\tau$	0
Ψ_{eff}^{A2}	$\lambda_1\, S_-^\tau$	$-\lambda_4\, S_-^\tau$	0	$\lambda_{3/3}^z\, S_z$	0	$\lambda_{3/3}\, S_+^\tau$
Ψ_{eff}^{B2}	$\lambda_4\, S_+^\tau$	$-\lambda_1\, S_+^\tau$	$-\lambda_{3/3}\, S_-^\tau$	0	$-\lambda_{3/3}^z\, S_z$	0
Ψ_{eff}^{A3}	$\lambda_3\, S_+^\tau$	$-\lambda_2\, S_+^\tau$	0	$\lambda_{3/3}\, S_-^\tau$	0	$\lambda_{3/3}^z\, S_z$

SOC. The remaining two SOC parameters, $\lambda_{1/2}$ and $\lambda_{3/3}^z$, are proportional to $V_{pd\pi}^2$ and describe in-plane SOC.

The physical meaning of these SOC parameters is probably more transparent if one rotates H_{so}^{ABC} into the basis of on-site effective p_z orbitals (see Appendix B 1). These basis vectors result from the admixture of an on-site p_z orbital $|\Psi_{1,0}^{\alpha j}\rangle$ with large weight and $|\Psi_{2,\pm1}^{\alpha' j}\rangle$, $|\Psi_{2,0}^{\alpha j}\rangle$ ($\alpha \neq \alpha'$) with small weight. H_{so}^{ABC} in the on-site effective p_z basis is shown in Table II. The SOC parameters $\lambda_1, \lambda_2, \lambda_3$, and λ_4 are linear combinations of $\lambda_{1/3}^{E_1}$, $\lambda_{1/3}^{E_2}$, $\lambda_{2/3}^{E_1}$, and $\lambda_{2/3}^{E_2}$, the explicit relations are given in Sec. V. In Sec. V we will also make predictions which might be useful to guide the fitting procedure if results of DFT calculations are fitted with a TB model, as, e.g., in Ref. 40.

Since the lattice of Bernard stacked bilayer graphene has the same symmetry group as ABC trilayer, the considerations made in this section can be easily applied to bilayer graphene as well. A brief summary of the bilayer calculations is given in Sec. IV. The importance of the bilayer results is that they can be compared with the numerical calculations of Ref. 40. Based on this comparison we will be able to estimate the values of five of the seven SOC parameters of ABC trilayer.

IV. INTRINSIC SOC IN BILAYER GRAPHENE

In this section we give a brief summary of our TB calculations for the intrinsic SOC in bilayer graphene and compare the results to the DFT computations of Ref. 40. The low-energy states of bilayer are also found at the K and K' points of the BZ; hence the calculation follows the same steps as in Sec. III: (i) First we obtain the basis states of the symmetry basis $\{|\Psi_{\Gamma_{A_1}}\rangle, |\Psi_{\Gamma_{A_2}}\rangle, |\Psi_{\Gamma_{E_{1,1}}}\rangle, |\Psi_{\Gamma_{E_{1,2}}}\rangle\}$, and (ii) we calculate the matrix elements of $\hat{H}_{SO}^{\text{atomic}}$. Note that in the case of bilayer graphene there is only one pair of bands which transforms as the two-dimensional representation Γ_E.

For easier comparison we adopt the notation of Ref. 40 for the SOC parameters. As is shown in Table III, the SO

TABLE III. Intrinsic spin-orbit Hamiltonian τH_{so}^{AB} of bilayer graphene in the basis of effective p_z orbitals.

SOC	Ψ_{eff}^{A1}	Ψ_{eff}^{B1}	Ψ_{eff}^{A2}	Ψ_{eff}^{B2}
Ψ_{eff}^{A1}	$\lambda_{\text{I2}}\, S_z$	$\lambda_0\, S_-^\tau$	$\lambda_4^{bi}\, S_+^\tau$	0
Ψ_{eff}^{B1}	$\lambda_0\, S_+^\tau$	$-\lambda_{\text{I1}}\, S_z$	0	$-\lambda_4^{bi}\, S_+^\tau$
Ψ_{eff}^{A2}	$\lambda_4^{bi}\, S_-^\tau$	0	$\lambda_{\text{I1}}\, S_z$	$-\lambda_0\, S_-^\tau$
Ψ_{eff}^{B2}	0	$-\lambda_4^{bi}\, S_-^\tau$	$-\lambda_0\, S_+^\tau$	$-\lambda_{\text{I2}}\, S_z$

Hamiltonian in the basis of the effective p_z orbitals can be written in a form which, apart from a unitary transformation, agrees with the result given in Table IV of Ref. 40 (see Appendix A for details). In terms of the SK hoppings, the SOC parameters read

$$\lambda_0 = 3\sqrt{3}\, \xi_d\, \frac{V_{pd\pi} V_{pd\sigma}}{\delta\varepsilon_{pd}^2 - \tilde{\gamma}_1^2}\, \frac{\tilde{\gamma}_1}{\varepsilon_{pd}}, \qquad \lambda_{\text{I1}} = \frac{9}{2}\, \xi_d\, \frac{V_{pd\pi}^2}{\delta\varepsilon_{pd}^2},$$

$$\lambda_4^{bi} = 3\sqrt{3}\, \xi_d\, \frac{V_{pd\pi} V_{pd\sigma}}{\delta\varepsilon_{pd}^2 - \tilde{\gamma}_1^2}, \qquad \lambda_{\text{I2}} = \frac{9}{2}\, \xi_d\, \frac{V_{pd\pi}^2}{\delta\varepsilon_{pd}^2 - \gamma_1^2}, \tag{8}$$

where $\tilde{\gamma}_1 = \gamma_1 + V_{dd\sigma}$. Looking at the expressions given in (8), one can make the following observations: (i) Since $\delta\varepsilon_{pd} = \varepsilon_p - \varepsilon_d < 0$ and $\tilde{\gamma}_1 > 0$, one can expect that the sign of λ_0 and λ_4^{bi} will be different; (ii) $|\lambda_0| < |\lambda_4^{bi}|$ because $\frac{\tilde{\gamma}_1}{|\varepsilon_{pd}|} < 1$; (iii) λ_{I1} and λ_{I2} have the same sign and they are approximately of the same magnitude because $\gamma_1^2/\delta\varepsilon_{pd}^2 \ll 1$.

By fitting the band structure obtained from DFT calculations with their tight-binding model, the authors of Ref. 40 found the following values for the bilayer SOC parameters: $2\lambda_{\text{I1}} = 24$ μeV, $2\lambda_{\text{I2}} = 20$ μeV, $\lambda_0 = 5$ μeV, $\lambda_4 = -12$ μeV. These numbers are in qualitative agreement with the predictions that we made below Eq. (8) for the SOC parameters. If, in addition, one assumes that $V_{pd\pi} V_{pd\sigma} < 0$ then according to (8) three of the parameters ($\lambda_{\text{I1}}, \lambda_{\text{I2}}, \lambda_0$) should have the same sign, which would again agree with the results of Ref. 40.

V. SOC PARAMETERS FOR TRILAYER GRAPHENE IN TERMS OF SK HOPPINGS

We are now ready to make predictions for five of the seven ABC trilayer SOC parameters. To this end, we first express the SOC parameters in the effective p_z orbital basis in terms of the SOC parameters obtained in the symmetry basis. Moreover, using the formulas given in Table IV for $\lambda_{1/3}^{E_1}, \lambda_{1/3}^{E_2}, \lambda_{2/3}^{E_1}$, and $\lambda_{2/3}^{E_2}$, one can also express $\lambda_1, \lambda_2, \lambda_3$, and λ_4 in terms of the SK hoppings. Taking into account the results of the previous section, this then facilitates making predictions for the numerical values of the ABC trilayer SOC parameters.

First, the SOC parameters in terms of the SK hoppings:

$$\lambda_1 = \left(\lambda_{1/3}^{E_1} + \lambda_{2/3}^{E_2} - \lambda_{1/3}^{E_2} - \lambda_{2/3}^{E_1}\right)/2$$
$$\approx \eta\left(-V_{pd\sigma} + \tilde{V}_{pd\sigma}\frac{\gamma_2}{\delta\varepsilon_{pd}}\right), \tag{9a}$$

$$\lambda_2 = \left(\lambda_{1/3}^{E_1} + \lambda_{1/3}^{E_2} - \lambda_{2/3}^{E_1} - \lambda_{2/3}^{E_2}\right)/2$$
$$\approx \eta\left(V_{pd\sigma}\frac{\gamma_1}{\delta\varepsilon_{pd}} + \tilde{V}_{pd\sigma}\frac{\gamma_2}{\delta\varepsilon_{pd}}\right), \tag{9b}$$

$$\lambda_3 = \left(\lambda_{1/3}^{E_1} + \lambda_{1/3}^{E_2} + \lambda_{2/3}^{E_1} + \lambda_{2/3}^{E_2}\right)/2$$
$$\approx \eta\left(V_{pd\sigma}\frac{\gamma_1}{\delta\varepsilon_{pd}}\frac{\gamma_2}{\delta\varepsilon_{pd}} + \tilde{V}_{pd\sigma}\right), \tag{9c}$$

$$\lambda_4 = \left(\lambda_{1/3}^{E_1} + \lambda_{1/3}^{E_2} + \lambda_{2/3}^{E_1} + \lambda_{2/3}^{E_2}\right)/2$$
$$\approx \eta\left(V_{pd\sigma}\frac{\gamma_2}{\delta\varepsilon_{pd}} + \tilde{V}_{pd\sigma}\frac{\gamma_1}{\delta\varepsilon_{pd}}\right), \tag{9d}$$

TABLE IV. Symmetry basis functions (left column) and intrinsic spin-orbit matrix elements (right column) in terms of Slater-Koster parameters. Here ξ_d is the angular momentum resolved atomic SOC strength, $V_{dd\sigma} = V_{dd\sigma}^{A1,B3}$, $\tilde{V}_{pd\sigma} = V_{pd\sigma}^{A1,B3}$, $V_{pd\sigma} = V_{pd\sigma}^{A2,B1} = V_{pd\sigma}^{A3,B2}$, $\delta\varepsilon_{pd} = \varepsilon_p - \varepsilon_d$, $\tilde{\gamma}_2 = \gamma_2 + V_{dd\sigma}$, and we assumed that $V_{pd\pi} = V_{pd\pi}^{Ai,Bi}$, $i = 1,2,3$. Although the basis functions shown in the right are not normalized, the SOC parameters are correct in the lowest order of the products of the small parameters $\tilde{V}_{pd\sigma}/(\delta\varepsilon_{pd} \pm \tilde{\gamma}_2)$, $V_{pd\sigma}/(\delta\varepsilon_{pd} \pm \gamma_2)$, $V_{pd\pi}/(\delta\varepsilon_{pd} \pm \gamma_1)$

$$|\Psi_{\Gamma_{A_1}}\rangle = |\overline{\Psi_{1,0,0}^{1,3}}\rangle + \frac{3}{\sqrt{2}}\frac{V_{pd\pi}}{\delta\varepsilon_{pd}-\gamma_2}|\overline{\Psi_{2,1,-1}^{3,1}}\rangle + \frac{\tilde{V}_{pd\sigma}}{\delta\varepsilon_{pd}-\tilde{\gamma}_2}|\Psi_{2,0,0}^{1,3}\rangle$$

$$\lambda_{1/2} = -\frac{9}{2}\xi_d\frac{(V_{pd\pi})^2}{(\delta\varepsilon_{pd}+\gamma_2)(\delta\varepsilon_{pd}-\gamma_2)}$$

$$|\Psi_{\Gamma_{A_2}}\rangle = |\Psi_{1,0,0}^{1,3}\rangle - \frac{3}{\sqrt{2}}\frac{V_{pd\pi}}{\delta\varepsilon_{pd}+\gamma_2}|\overline{\Psi_{2,1,-1}^{3,1}}\rangle - \frac{\tilde{V}_{pd\sigma}}{\delta\varepsilon_{pd}+\tilde{\gamma}_2}|\overline{\Psi_{2,0,0}^{1,3}}\rangle$$

$$\lambda_{1/3}^{E_1} = \frac{3\sqrt{3}}{2}\xi_d\frac{V_{pd\pi}}{(\delta\varepsilon_{pd}+\gamma_1)}\left(\frac{\tilde{V}_{pd\sigma}}{\delta\varepsilon_{pd}-\tilde{\gamma}_2} - \frac{V_{pd\sigma}}{\delta\varepsilon_{pd}-\gamma_2}\right)$$

$$|\Psi_{\Gamma_{E_{1,1}}}\rangle = |\Psi_{1,0,0}^{2,1}\rangle + \frac{1}{\delta\varepsilon_{pd}+\gamma_1}\left[\frac{V_{pd\sigma}}{\sqrt{2}}|\overline{\Psi_{2,0,0}^{2,1}}\rangle - \frac{3V_{pd\pi}}{2}|\overline{\Psi_{2,1,-1}^{1,2}}\rangle\right]$$

$$\lambda_{1/3}^{E_2} = \frac{3\sqrt{3}}{2}\xi_d\frac{V_{pd\pi}}{(\delta\varepsilon_{pd}-\gamma_1)}\left(\frac{\tilde{V}_{pd\sigma}}{\delta\varepsilon_{pd}-\tilde{\gamma}_2} + \frac{V_{pd\sigma}}{\delta\varepsilon_{pd}-\gamma_2}\right)$$

$$|\Psi_{\Gamma_{E_{1,2}}}\rangle = |\Psi_{1,0,0}^{3,2}\rangle + \frac{1}{\delta\varepsilon_{pd}+\gamma_1}\left[\frac{V_{pd\sigma}}{\sqrt{2}}|\overline{\Psi_{2,0,0}^{3,2}}\rangle - \frac{3V_{pd\pi}}{2}|\overline{\Psi_{2,1,-1}^{2,3}}\rangle\right]$$

$$\lambda_{2/3}^{E_1} = \frac{3\sqrt{3}}{2}\xi_d\frac{V_{pd\pi}}{(\delta\varepsilon_{pd}+\gamma_1)}\left(\frac{\tilde{V}_{pd\sigma}}{\delta\varepsilon_{pd}+\tilde{\gamma}_2} + \frac{V_{pd\sigma}}{\delta\varepsilon_{pd}+\gamma_2}\right)$$

$$|\Psi_{\Gamma_{E_{2,1}}}\rangle = |\overline{\Psi_{1,0,0}^{2,1}}\rangle + \frac{1}{\delta\varepsilon_{pd}-\gamma_1}\left[\frac{3V_{pd\pi}}{2}|\Psi_{2,1,-1}^{1,2}\rangle - \frac{V_{pd\sigma}}{\sqrt{2}}|\Psi_{2,0,0}^{2,1}\rangle\right]$$

$$\lambda_{2/3}^{E_2} = \frac{3\sqrt{3}}{2}\xi_d\frac{V_{pd\pi}}{(\delta\varepsilon_{pd}-\gamma_1)}\left(\frac{\tilde{V}_{pd\sigma}}{\delta\varepsilon_{pd}+\tilde{\gamma}_2} - \frac{V_{pd\sigma}}{\delta\varepsilon_{pd}+\gamma_2}\right)$$

$$|\Psi_{\Gamma_{E_{2,2}}}\rangle = |\overline{\Psi_{1,0,0}^{3,2}}\rangle + \frac{1}{\delta\varepsilon_{pd}-\gamma_1}\left[\frac{3V_{pd\pi}}{2}|\Psi_{2,1,-1}^{2,3}\rangle - \frac{V_{pd\sigma}}{\sqrt{2}}|\Psi_{2,0,0}^{3,2}\rangle\right]$$

$$\lambda_{3/3} = 3\sqrt{3}\xi_d\frac{V_{pd\pi}V_{pd\sigma}}{(\delta\varepsilon_{pd}+\gamma_1)(\delta\varepsilon_{pd}-\gamma_1)}$$

$$\lambda_{3/3}^z = -\frac{9}{2}\xi_d\frac{(V_{pd\pi})^2}{(\delta\varepsilon_{pd}+\gamma_1)(\delta\varepsilon_{pd}-\gamma_1)}$$

where $\eta = 3\sqrt{3}\xi_d\frac{V_{pd\pi}}{\delta\varepsilon_{pd}^2-\gamma_1^2}$. Similarly to the bilayer case, looking at Table IV and Eqs. (9) one can make the following observations: (i) One would expect that $\lambda_{1/2} \approx \lambda_{3/3}^z$, (ii) $|\lambda_{3/3}| \approx |\lambda_1|$ and assuming that $V_{pd\sigma}/\tilde{V}_{pd\sigma} \propto \gamma_1/\gamma_2$ one finds that $|\lambda_1| > |\lambda_2| > |\lambda_3| > |\lambda_4|$, and (iii) λ_4 has opposite sign from λ_3 and similarly for $\lambda_{3/3}$ and λ_1 because the second term in the expression for λ_1 in Eq. (9a) can be neglected with respect to the first one.

Comparing the expressions in terms of the SK hoppings given in Eqs. (9) with the corresponding ones for the bilayer case in (8), the following estimates can be made: $2\lambda_{1/2}^z \approx 2\lambda_{3/3}^z \approx 20\ \mu$eV, $|\lambda_{3/3}| \approx |\lambda_1| \approx 10\ \mu$eV, and $|\lambda_2| \approx 5\ \mu$eV. Since λ_3 and λ_4 are proportional to $\tilde{V}_{pd\sigma}$ (assuming $V_{pd\sigma}/\tilde{V}_{pd\sigma} \propto \gamma_1/\gamma_2$) which is unknown, we cannot give a numerical estimate for their value. One would expect that they are much smaller than λ_1 and λ_2 because $\tilde{V}_{pd\sigma}$ corresponds to a remote, and presumably weak p-d hopping between the A1 and B3 sites.

VI. EFFECTIVE SOC HAMILTONIAN

The calculations in the previous sections are valid, strictly speaking, only at the K point of the Brillouin zone. To obtain the Hamiltonian in the vicinity of the K point, where the states close to the Fermi energy can be found, one can perform a $\mathbf{k} \cdot \mathbf{p}$ expansion of the bands. We neglect the weak $\mathbf{k}$ dependence of the SOC;[40] hence the total Hamiltonian of the system can be written as $\hat{H}_{ABC} = \hat{H}_{\mathbf{k} \cdot \mathbf{p}}^{ABC} + \tau\,\hat{H}_{so}^{ABC}$. Here $\hat{H}_{\mathbf{k} \cdot \mathbf{p}}^{ABC}$ is the $\mathbf{k} \cdot \mathbf{p}$ Hamiltonian obtained without taking into account the SOC, whereas $\hat{H}_{so}^{ABC}$ is the SOC Hamiltonian calculated at the K point. $\hat{H}_{so}^{ABC}$ has been published before; see, e.g., Refs. 8 and 11.

To study the low-energy physics, however, in which we are primarily interested, the use of $\hat{H}_{\mathbf{k} \cdot \mathbf{p}}^{ABC}$ is not convenient, since it includes four bands that are split off from the Fermi energy of the (undoped) ABC trilayer by the large energy scale $\approx \pm\gamma_1$.[8,11] Therefore we derive an effective two-component (or, including the spin, four-component) Hamiltonian $\hat{H}_{ABC}^{\text{eff}}$ which

describes the hopping between atomic sites A1 and B3. To this end we again employ the Schrieffer-Wolff transformation and keep all terms which are third order or less in the momentum π, $\pi^\dagger$ and first order in the SOC constants. Here $\pi = -(ip_x + \tau p_y)$, where $\tau = 1\ (-1)$ for valley $K\ (K')$ and the momenta p_x, p_y are measured from the $K\ (K')$ point of the BZ; see Fig. 1(c). Keeping terms up to third order in π, $\pi^\dagger$ is essential to reproduce the important features of the low-energy band structure,[8,11] such as the band degeneracy and the trigonal warping. The necessary formulas for the matrix elements of the effective Hamiltonian can be found in Ref. 46. We treat γ_1 as a large energy scale with respect to $v_0\pi$, $|\gamma_3|$, γ_4, γ_2 and the typical energies E we are interested in and keep only the leading order for the terms involving γ_2, v_3, and v_4. [The velocities v_i are given by $v_i = (\sqrt{3}/2)a\gamma_i/\hbar$, where $a = 0.246$ nm is the lattice constant of graphene.] For the folding down of the full Hamiltonian we use the form of $\hat{H}_{ABC}$ in the symmetry basis because in this case all the large matrix elements are on the diagonal and therefore the quasidegenerate perturbation approach is expected to work well. Once we obtain the effective Hamiltonian $\hat{H}_{ABC}^{\text{eff}}$ in the symmetry basis we rotate it into the basis of effective p_z orbitals centered on atomic sites A1 and B3 because $\hat{H}^{\text{eff}}$ assumes a simpler form in this basis. Explicitly, one can write $\hat{H}_{ABC}^{\text{eff}} = \hat{H}_{el}^{\text{eff}} + \hat{H}_{so}^{\text{eff}}$, where the electronic part is given by

$$\hat{H}_{el}^{\text{eff}} = \hat{H}_{\text{chir}} + \hat{H}_{3w} + \hat{H}_{\gamma_2} + \hat{H}_{v_4},$$

$$\hat{H}_{\text{chir}} = \frac{v_0^3}{\gamma_1^2}\begin{pmatrix} 0 & (\pi^\dagger)^3 \\ \pi^3 & 0 \end{pmatrix}, \tag{10a}$$

$$\hat{H}_{3w} = -\frac{v_0 v_3}{\gamma_1}[\pi^\dagger\pi + \pi\pi^\dagger]\begin{pmatrix} 0 & 1 \\ 1 & 0 \end{pmatrix}, \tag{10b}$$

$$\hat{H}_{\gamma_2} = \gamma_2\left(1 - \frac{1}{2}\frac{v_0^2}{\gamma_1^2}[\pi^\dagger\pi + \pi\pi^\dagger]\right)\begin{pmatrix} 0 & 1 \\ 1 & 0 \end{pmatrix}, \tag{10c}$$

$$\hat{H}_{v_4} = -\frac{2v_0 v_4}{\gamma_1}\begin{pmatrix} \pi^\dagger\pi & 0 \\ 0 & \pi\pi^\dagger \end{pmatrix}. \tag{10d}$$

We note that when applying the Schrieffer-Wolff transformation we did not assume that π and $\pi^\dagger$ commute; therefore the Hamiltonians (10) and (11) are valid *in the presence of finite external magnetic field* as well. In zero magnetic field, using the notation $p^2 = \pi\pi^\dagger = \pi^\dagger\pi$, the Hamiltonian (VI) simplifies to the corresponding results in Refs. 8 and 11.

The effective SOC Hamiltonian is

$$\hat{H}_{so}^{\rm eff} = \hat{H}_{so}^{mn} + \hat{H}_{so}^{(1)} + \hat{H}_{so}^{(2)} + \hat{H}_{so}^{(3)},$$

$$\hat{H}_{so}^{mn} = \tau\,\lambda_{1/2} S_z \sigma_z, \tag{11a}$$

$$\hat{H}_{so}^{(1)} = -\tau\,\tilde{\lambda}_1 \frac{v_0}{\gamma_1}[S_-^\tau \pi^\dagger + S_+^\tau \pi]\sigma_z, \tag{11b}$$

$$\hat{H}_{so}^{(2)} = \tau\,\frac{v_0 v_3}{\gamma_1^2}\lambda_{3/3}[S_+^\tau(\pi^\dagger)^2 + S_-^\tau \pi^2]\sigma_z, \tag{11c}$$

$$\hat{H}_{so}^{(3)} = -\tau\,\frac{v_0^2}{\gamma_1^2}(\lambda_{3/3}^z - \lambda_{1/2})S_z\begin{pmatrix} \pi^\dagger\pi & 0 \\ 0 & -\pi\pi^\dagger \end{pmatrix}. \tag{11d}$$

Here the Pauli matrix σ_z acts in the space of {A1,B3} sites and $\tilde{\lambda}_1 = \lambda_1 + \lambda_3(v_3/v_0) + \lambda_2(v_4/v_0) \approx \lambda_1$. At low energies $v_0^2 p^2, v_0 v_3 p^2 \ll \gamma_1^2$ and the corresponding terms in (11d) can be neglected. The first term, $\hat{H}_{so}^{(mn)}$, is the well-known SO Hamiltonian of monolayer graphene[35] and describes the leading contribution to SOC. The next term, $\hat{H}_{so}^{(1)}$, is the most important momentum-dependent contribution close to the K point. Keeping only $\hat{H}_{so}^{(mn)}$ and $\hat{H}_{so}^{(1)}$ the effective SOC Hamiltonian can be written in a more compact form as

$$\hat{H}_{so}^{\rm eff} = \tau\left[\lambda_{1/2} S_z + \tilde{\lambda}_1 \frac{v_0}{\gamma_1}(\mathbf{S}\times\mathbf{p})_z\right]\sigma_z, \tag{12}$$

where $\mathbf{p} = (p_x, p_y)$. We note that Eq. (12) also describes the effective SOC Hamiltonian of bilayer graphene with $\lambda_{1/2}$ replaced by $-\lambda_{\rm I1}$ and $\tilde{\lambda}_1 = -\lambda_4^{bi} + \lambda_0(v_4/v_0) \approx -\lambda_4^{bi}$ (for $\lambda_{\rm I1}$, λ_0, and λ_4^{bi} see Sec. IV).

In zero external magnetic field $\hat{H}_{ABC}^{\rm eff}$ is easily diagonalizable. Keeping only the leading terms (12) in $\hat{H}_{so}^{\rm eff}$, we obtain the eigenvalues $E_\pm = -2\frac{v_0 v_4}{\gamma_1}p^2 \pm r(\mathbf{p})$ (each doubly degenerate), where $r(\mathbf{p}) = \sqrt{\lambda_{1/2}^2 + |c(\mathbf{p})|^2 + |d(\mathbf{p})|^2}$, $c(\mathbf{p}) = -\tilde{\lambda}_1\frac{v_0}{\gamma_1}pe^{i\phi_\mathbf{p}}$, $d(\mathbf{p}) = \gamma_2 - \frac{2v_0 v_3}{\gamma_1}p^2 + \frac{v_0^3}{\gamma_1^2}p^3 e^{-3i\phi_\mathbf{p}}$ (where $p = |\pi|$), whereas $\phi_\mathbf{p}$ is the phase of π. The main effect of SOC on the spectrum is, similarly to monolayer[35] and bilayer[30,40] graphene, to open a band gap $E_{bg} = 2\sqrt{\lambda_{1/2}^2 + |c(\mathbf{p}_d)|^2}$ at the band degeneracy points $\mathbf{p}_d$, while preserving the spin degeneracy of the bands (see Fig. 2). Comparing E_{bg} to the SOC band gap in monolayer and bilayer graphene at the K point, we expect that in ABC trilayer it should be somewhat bigger due to the $|c(\mathbf{p}_d)|^2$ term, i.e., because the band gap can be found away from the K point at finite $\mathbf{p}_d$. In Fig. 2 we compare the low-energy bands calculated using the full Hamiltonian (which includes the high-energy bands as well) and using the effective Hamiltonian $\hat{H}_{ABC}^{\rm eff}$. From this, we conclude that the effective theory represents a good approximation.

VII. SUBSTRATE INDUCED SOC

The calculations of Secs. III–V suggest that the intrinsic SOC in ABC trilayer is relatively small; the order of magnitude of the SOC parameters is 10 μeV, the same
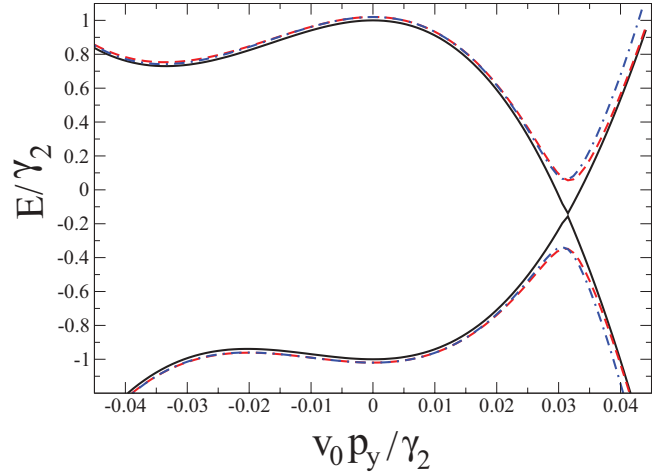

FIG. 2. (Color online) Low-energy bands of ABC trilayer graphene at the K point as a function of p_y for $p_x = 0$: using the full $\mathbf{k}\cdot\mathbf{p}$ Hamiltonian with zero spin-orbit coupling (solid black), with finite spin-orbit coupling (red dashed), and using the effective Hamiltonian $\hat{H}_{ABC}^{\rm eff}$ (dashed-dotted blue). The parameters v_i were taken from Ref. 11 and we have chosen $\lambda_{1/2} = \lambda_1 = 0.2\,\gamma_2$.

as in monolayer[37–39,44] or bilayer[40] graphene. One can, in principle, enhance the SOC in a number of ways, e.g., by impurities,[51] by applying strong external electric field,[40] making the graphene sheet curved,[52] using adatoms with large atomic number,[53–55] or bringing the trilayer into proximity with a suitable substrate.[56,57] Since proximity to a substrate or adatoms is likely to lead to a larger SOC effect than what one can induce by an external electric field, here we consider an effective model whereby strong SOC is induced in one of the outer layers of trilayer graphene whereas SOC is not altered in the other two layers. For concreteness, we assume that it is the first graphene layer where strong SOC is induced and for simplicity we will refer both to the scenario involving a substrate and that involving adatoms as "substrate induced SOC." From the symmetry point of view, the model we consider here is not exact: A group-theoretical analysis[40,42,43] of the matrix elements of the SOC Hamiltonian shows that by breaking the inversion symmetry there can be in principle 21 different SOC parameters. However, we assume that all intra- and interlayer SOC parameters will remain small with respect to the SOC parameters in the layer that is in the immediate proximity of the substrate. The relevant part of the SOC Hamiltonian that we consider as a minimal model is shown in Table V. We assume that at the K point of the BZ only four SOC parameters have significant values and neglect all other intra- or interlayer coupling spin-orbit parameters. The

TABLE V. The nonzero part of the model SOC Hamiltonian $\tau\,\tilde{H}_{so}^{\rm ext}$.

SOC	$\Psi_{\rm eff}^{A1}$	$\Psi_{\rm eff}^{B3}$	$\Psi_{\rm eff}^{B1}$
$\Psi_{\rm eff}^{A1}$	$\tilde{\lambda}_{1/2}S_z$	0	$\lambda_{BR}S_+^\tau$
$\Psi_{\rm eff}^{B3}$	0	$-\lambda_{1/2}S_z$	0
$\Psi_{\rm eff}^{B1}$	$\lambda_{BR}S_-^\tau$	0	$-\tilde{\lambda}_{3/3}^z S_z$

SOC parameters that we keep are $\tilde{\lambda}_{1/2}$ and $\tilde{\lambda}^z_{3/3}$ which may describe enhanced diagonal SOC on A1- and B1-type atoms, respectively, whereas λ_{BR} is the Bychkov-Rashba[58] type SOC acting only in the first graphene layer. Since we are going to derive an effective low-energy Hamiltonian, we also keep nonzero the intrinsic SOC parameter $\lambda_{1/2}$ on atom B3, which, however, might be much smaller than $\tilde{\lambda}_{1/2}$ and $\tilde{\lambda}^z_{3/3}$.

Similarly to Sec. VI, for the full Hamiltonian of the system in the vicinity of the K point we take $\tilde{H}_{ABC} = \tilde{H}^{ABC}_{\mathbf{k \cdot p}} + \tilde{H}^{ext}_{so}$. In the Hamiltonian $\tilde{H}^{ABC}_{\mathbf{k \cdot p}}$, as an additional substrate effect, we also include a possible shift Δ of the on-site energies of atoms A1 and B1 with respect to atoms in the other two layers. (Otherwise $\tilde{H}^{ABC}_{\mathbf{k \cdot p}}$ is the same as in Sec. VI.) To study the low-energy physics we again use the Schrieffer-Wolff transformation to eliminate the high-energy bands. The hopping γ_1 is treated as a large energy scale with respect to $v_0\pi$, $|\gamma_3|$, γ_4, γ_2, Δ and we keep only the leading order for the terms involving Δ, γ_2, v_3, and v_4. The electronic part $\hat{\tilde{H}}^{eff}_{el}$ of the effective Hamiltonian $\hat{\tilde{H}}^{eff}_{ABC}$ contains one new term in addition to the terms in Eq. (10):

$$\hat{H}_\Delta = \Delta \left[\begin{pmatrix} 1 & 0 \\ 0 & 0 \end{pmatrix} - \frac{v_0^2}{2\gamma_1^2} \begin{pmatrix} 2\pi^\dagger\pi + \pi\pi^\dagger & 0 \\ 0 & -\pi\pi^\dagger \end{pmatrix} \right]. \quad (13)$$

Up to linear order in the momentum and the SOC parameters the effective spin-orbit Hamiltonian has the following terms:

$$\hat{H}^{ABC}_{so} = \left[\hat{H}^{ABC,(0)}_{so} + \hat{H}^{ABC,(1)}_{so} + \hat{H}^{ABC,(2)}_{so} \right],$$

$$\hat{H}^{ABC,(0)}_{so} = \tau \, S_z \begin{pmatrix} \tilde{\lambda}_{1/2} & 0 \\ 0 & -\lambda_{1/2} \end{pmatrix}, \quad (14a)$$

$$\hat{H}^{ABC,(1)}_{so} = -\tau \, \lambda_{BR} \frac{v_3}{\gamma_1} \begin{pmatrix} 0 & S^\tau_+\pi \\ S^\tau_-\pi^\dagger & 0 \end{pmatrix}, \quad (14b)$$

$$\hat{H}^{ABC,(2)}_{so} = -\tau \, \lambda_{BR} \frac{v_4}{\gamma_1}(S^\tau_-\pi^\dagger + S^\tau_+\pi) \begin{pmatrix} 1 & 0 \\ 0 & 0 \end{pmatrix}. \quad (14c)$$

It is interesting to compare this result to what one obtains for bilayer graphene using the same model:[59]

$$\hat{H}^{AB}_{so} = \tau \cdot \left[\hat{H}^{AB,(0)}_{so} + \hat{H}^{AB,(1)}_{so} + \hat{H}^{AB,(2)}_{so} \right],$$

$$\hat{H}^{AB,(0)}_{so} = S_z \begin{pmatrix} \tilde{\lambda}^z_{3/3} & 0 \\ 0 & -\lambda^z_{3/3} \end{pmatrix}, \quad (15a)$$

$$\hat{H}^{AB,(1)}_{so} = -\lambda_{BR} \frac{v_0}{\gamma_1} \begin{pmatrix} 0 & S^\tau_+\pi^\dagger \\ S^\tau_-\pi & 0 \end{pmatrix}, \quad (15b)$$

$$\hat{H}^{AB,(2)}_{so} = -\lambda_{BR} \frac{v_4}{\gamma_1}(S^\tau_-\pi^\dagger + S^\tau_+\pi) \begin{pmatrix} 1 & 0 \\ 0 & 0 \end{pmatrix}. \quad (15c)$$

In the appropriate limit Hamiltonian (15) agrees with the result of Ref. 40. Similar models have also been considered in two recent works: In Ref. 61 strong Rashba SOC was assumed in both layers of bilayer graphene and a linear-in-momentum low-energy SOC Hamiltonian was derived, whereas in

Ref. 60 the authors kept only the first term, $\hat{H}^{AB,(0)}_{so}$, and set $\lambda^z_{3/3} = 0$.

One can see that in contrast to monolayer graphene, in bilayer and ABC trilayer graphene the Rashba SOC affects the spin dynamics in the low-energy bands through terms which are momentum dependent.[62] This means that at the K (K') point the effect of Rashba-type SOC is suppressed with respect to monolayer graphene. Furthermore, noting that $v_0 \gg v_3$, a comparison of the prefactors of $\hat{H}^{ABC,(1)}_{so}$ and $\hat{H}^{AB,(1)}_{so}$ may suggest that the influence of linear-in-momentum terms on spin dynamics might be more important in bilayer than in trilayer. This is, strictly speaking, only true in the model that we used, i.e., when other off-diagonal SOC parameters can be neglected with respect to λ_{BR}. In general, there would be a linear-in-momentum SOC Hamiltonian with a prefactor proportional to v_0/γ_1 for the trilayer case as well. The model introduced above could be relevant, e.g., in an experiment similar to Ref. 57 if bilayer or trilayer is used instead of monolayer graphene. Varykhalov *et al.*[57] reported a large Rashba SOC in monolayer graphene with λ_{BR} between 10–100 meV, whereas, as we have seen, the intrinsic SOC parameters are typically of a few 10 μeV.

A detailed study of the properties of Hamiltonians (14) and (15) is left for a future study. We expect a rich physics emerging from the interplay of diagonal and off-diagonal spin-orbit terms and the interlayer asymmetry Δ.

VIII. CONCLUSIONS

In conclusion, we studied the intrinsic and substrate induced spin-orbit interaction in bilayer and ABC trilayer graphene. Assuming that in flat graphene systems the most important contribution to the SOC comes from the admixture of p_z and d orbitals and using a combination of group-theoretical and tight-binding approaches, we derived the intrinsic SOC Hamiltonian of ABC trilayer graphene. In contrast to the similar calculations for monolayer graphene,[39] we found that

TABLE VI. Character table of the group 32 (D_3).

32 (D_3)	E	$2C_3$	$3C_2$
Γ_{A_1}	1	1	1
Γ_{A_2}	1	1	−1
Γ_E	2	−1	0

TABLE VII. Basis functions for the irreducible representations of the small group of the K point for ABC trilayer graphene. The basis functions for the K' point can be obtained by complex conjugation.

Γ_{A_1}	$\overline{\|\Psi^{1,3}_{1,0,0}\rangle}$, $\|\Psi^{3,1}_{2,1,-1}\rangle$, $\|\Psi^{1,3}_{2,0,0}\rangle$, $\|\Psi^{3,1}_{2,-2,2}\rangle$, $\|\Psi^{2,2}_{2,-1,1}\rangle$, $\|\Psi^{2,2}_{2,2,-2}\rangle$
Γ_{A_2}	$\|\Psi^{1,3}_{1,0,0}\rangle$, $\overline{\|\Psi^{3,1}_{2,1,-1}\rangle}$, $\overline{\|\Psi^{1,3}_{2,0,0}\rangle}$, $\overline{\|\Psi^{3,1}_{2,-2,2}\rangle}$, $\overline{\|\Psi^{2,2}_{2,-1,1}\rangle}$, $\overline{\|\Psi^{2,2}_{2,2,-2}\rangle}$
Γ_E	$\{\|\Psi^{2,1}_{1,0,0}\rangle, \|\Psi^{3,2}_{1,0,0}\rangle\}$, $\{\overline{\|\Psi^{2,1}_{1,0,0}\rangle}, \overline{\|\Psi^{3,2}_{1,0,0}\rangle}\}$
	$\{\|\Psi^{A2}_{2,0}\rangle, \|\Psi^{B2}_{2,0}\rangle\}$, $\{\|\Psi^{A2}_{2,-1}\rangle, \|\Psi^{B2}_{2,1}\rangle\}$, $\{\|\Psi^{A2}_{2,-2}\rangle, \|\Psi^{B2}_{2,2}\rangle\}$
	$\{\|\Psi^{A3}_{2,0}\rangle, \|\Psi^{B1}_{2,0}\rangle\}$, $\{\|\Psi^{A3}_{2,-1}\rangle, \|\Psi^{B1}_{2,1}\rangle\}$, $\{\|\Psi^{A3}_{2,2}\rangle, \|\Psi^{B1}_{2,-2}\rangle\}$
	$\{\|\Psi^{A1}_{2,1}\rangle, \|\Psi^{B3}_{2,-1}\rangle\}$, $\{\|\Psi^{A1}_{2,-1}\rangle, \|\Psi^{B3}_{2,1}\rangle\}$, $\{\|\Psi^{A1}_{2,2}\rangle, \|\Psi^{B3}_{2,-2}\rangle\}$
	$\{\|\Psi^{A1}_{2,-2}\rangle, \|\Psi^{B3}_{2,2}\rangle\}$

TABLE VIII. The same as in Table VII but for bilayer graphene.

Γ_{A_1}	$\left|\overline{\Psi^{2,1}_{1,0,0}}\right\rangle, \left|\Psi^{1,2}_{2,1,-1}\right\rangle, \left|\Psi^{2,1}_{2,0,0}\right\rangle, \left|\Psi^{2,1}_{2,-2,2}\right\rangle$
Γ_{A_2}	$\left|\Psi^{2,1}_{1,0,0}\right\rangle, \left|\overline{\Psi^{1,2}_{2,1,-1}}\right\rangle, \left|\overline{\Psi^{2,1}_{2,0,0}}\right\rangle, \left|\overline{\Psi^{2,1}_{2,-2,2}}\right\rangle$
Γ_E	$\left\{\left|\Psi^{A1}_{1,0}\right\rangle, \left|\Psi^{B2}_{1,0}\right\rangle\right\}, \left\{\left|\Psi^{A1}_{2,0}\right\rangle, \left|\Psi^{B2}_{2,0}\right\rangle\right\}, \left\{\left|\Psi^{A1}_{2,-1}\right\rangle, \left|\Psi^{B2}_{2,1}\right\rangle\right\}$
	$\left\{\left|\Psi^{A1}_{2,2}\right\rangle, \left|\Psi^{B2}_{2,-2}\right\rangle\right\}, \left\{\left|\Psi^{A1}_{2,-2}\right\rangle, \left|\Psi^{B2}_{2,2}\right\rangle\right\}, \left\{\left|\Psi^{A2}_{2,-1}\right\rangle, \left|\Psi^{B1}_{2,1}\right\rangle\right\}$
	$\left\{\left|\Psi^{A2}_{2,1}\right\rangle, \left|\Psi^{B1}_{2,-1}\right\rangle\right\}, \left\{\left|\Psi^{A2}_{2,2}\right\rangle, \left|\Psi^{B1}_{2,-2}\right\rangle\right\}$

in bilayer and ABC trilayer in addition to d_{xz} and d_{yz} orbitals also d_{z^2} orbitals have to be taken into account. For both bilayer and trilayer graphene we obtained explicit expressions for the SOC parameters in terms of SK hopping parameters. By comparing these expressions with the DFT calculations of Ref. 40, we were able to estimate the values of the intrinsic SOC constants for ABC trilayer graphene. Since the intrinsic SOC is quite small, we considered a situation when adatoms or a substrate can induce a strong SOC (intrinsic diagonal or Rashba-type off-diagonal) in only one of the layers of bilayer and ABC trilayer graphene. To describe the low-energy physics we derived effective Hamiltonians for both systems. We found that the effect of Rashba-type SOC is suppressed close to the K (K') point with respect to monolayer graphene.

The approach that we used here to derive the SOC Hamiltonians can be employed in the case of other related problems as well. For instance ABA stacked trilayer graphene or graphite can be treated on the same footing when one takes into account that they have different symmetries from bilayer and ABC trilayer graphene. Considering the substrate induced SOC, which can be strong enough to make the SOC related phenomena experimentally observable, one interesting question is whether the different symmetries and band structure of ABC and ABA trilayer would manifest themselves in, e.g., significantly different spin-transport properties.

APPENDIX A: SMALL GROUP OF THE K POINT AND BASIS FUNCTIONS

The relevant symmetry group for the calculations at the K point for both trilayer and bilayer graphene is the group 32 (D_3). The generators of this group are two threefold rotations (C_3) around an axis perpendicular to the plane of the graphene

layers and three twofold rotations (C_2). There are three irreducible representations, two one-dimensional denoted by Γ_{A_1}, Γ_{A_2} and a two-dimensional one, Γ_E (see Table VI).

The basis functions built from the linear combinations of p_z and d orbitals which transform as these irreducible representations are shown in Table VII for ABC trilayer and in Table VIII for bilayer. In the case of bilayer, making then the same steps as for trilayer graphene, one finds the symmetry basis and intrinsic SOC parameters given in Table IX. Referring to Fig. 1(a), the atomic sites participating in the formation of the split-off bands are denoted by B1 and A2, whereas they are labeled as A1 and B2 in Ref. 40, and similarly for the sites contributing to the low-energy bands. Therefore, to arrive at the SOC Hamiltonian shown in Table III, (i) one has to rotate the symmetry basis into the on-site basis, (ii) relabel the sites as A$j \leftrightarrows$ Bj, (iii) and make the identification $\lambda_{I1} = -\lambda^z_{3/3}$, $\lambda_{I2} = -\lambda_{1/2}$, $\lambda_0 = \frac{1}{\sqrt{2}}(\lambda_{2/3} - \lambda_{1/3})$, $\lambda^{bi}_4 = -\frac{1}{\sqrt{2}}(\lambda_{2/3} + \lambda_{1/3})$. The matrix elements are real numbers in our calculations because we use different lattice vectors than in Ref. 40.

APPENDIX B

Here we collect some useful formulas: We give explicitly the transformation between the symmetry basis and the effective on-site p_z orbital basis for the trilayer case and present the low-energy electronic Hamiltonian for bilayer graphene.

1. Transformation between the symmetry basis and the on-site effective p_z basis

The transformation reads

$$\begin{pmatrix}|\Psi^{A1}_{\text{eff}}\rangle \\ |\Psi^{B3}_{\text{eff}}\rangle \\ |\Psi^{B1}_{\text{eff}}\rangle \\ |\Psi^{A2}_{\text{eff}}\rangle \\ |\Psi^{B2}_{\text{eff}}\rangle \\ |\Psi^{A3}_{\text{eff}}\rangle\end{pmatrix} = \frac{1}{\sqrt{2}} \begin{pmatrix} 1 & 1 & 0 & 0 & 0 & 0 \\ -1 & 1 & 0 & 0 & 0 & 0 \\ 0 & 0 & 1 & 0 & -1 & 0 \\ 0 & 0 & 1 & 0 & 1 & 0 \\ 0 & 0 & 0 & 1 & 0 & -1 \\ 0 & 0 & 0 & 1 & 0 & 1 \end{pmatrix} \begin{pmatrix}|\Psi_{\Gamma_{A_1}}\rangle \\ |\Psi_{\Gamma_{A_2}}\rangle \\ |\Psi_{\Gamma_{E_{1,1}}}\rangle \\ |\Psi_{\Gamma_{E_{1,2}}}\rangle \\ |\Psi_{\Gamma_{E_{2,1}}}\rangle \\ |\Psi_{\Gamma_{E_{2,2}}}\rangle\end{pmatrix}.$$

$$\tag{B1}$$

2. Bilayer graphene low-energy electronic Hamiltonian

For completeness and for comparison with the trilayer case given in Eq. (10), we show here the low-energy electronic Hamiltonian of bilayer graphene in the on-site basis A1, B2. This Hamiltonian has been discussed in many publications before; see, e.g., the recent review of Ref. 63. As in Sec. VII, we assume that atoms A1 and B1 in the layer adjacent to the

TABLE IX. Symmetry basis functions (left column) and intrinsic spin-orbit matrix elements (right column) in terms of Slater-Koster parameters for bilayer graphene. We used the notation $V_{pd\sigma} = V^{A2,B1}_{pd\sigma}$, $\delta\varepsilon_{pd} = \varepsilon_p - \varepsilon_d$, and $\tilde{\gamma}_1 = \gamma_1 + V_{dd\sigma}$.

$\left|\Psi_{\Gamma_{A_1}}\right\rangle = \left|\overline{\Psi^{2,1}_{1,0,0}}\right\rangle + \frac{3}{\sqrt{2}}\frac{V_{pd\pi}}{\delta\varepsilon_{pd}-\gamma_1}\left|\Psi^{1,2}_{2,1,-1}\right\rangle - \frac{V_{pd\sigma}}{\delta\varepsilon_{pd}-\tilde{\gamma}_1}\left|\Psi^{2,1}_{2,0,0}\right\rangle$	$\lambda_{1/2} = -\frac{9}{2}\xi_d \frac{(V_{pd\pi})^2}{\left(\delta\varepsilon^2_{pd}-\gamma^2_1\right)}$
$\left|\Psi_{\Gamma_{A_2}}\right\rangle = \left|\Psi^{2,1}_{1,0,0}\right\rangle - \frac{3}{\sqrt{2}}\frac{V_{pd\pi}}{\delta\varepsilon_{pd}+\gamma_1}\left|\overline{\Psi^{1,2}_{2,1,-1}}\right\rangle + \frac{V_{pd\sigma}}{\delta\varepsilon_{pd}+\tilde{\gamma}_1}\left|\overline{\Psi^{2,1}_{2,0,0}}\right\rangle$	$\lambda_{1/3} = -3\sqrt{\frac{3}{2}}\xi_d \frac{V_{pd\pi}V_{pd\sigma}}{\delta\varepsilon_{pd}(\delta\varepsilon_{pd}-\tilde{\gamma}_1)}$
$\left|\Psi_{\Gamma_{E_{1,1}}}\right\rangle = \left|\Psi^{A1}_{1,0}\right\rangle + \frac{3}{\sqrt{2}}\frac{V_{pd\pi}}{\delta\varepsilon_{pd}}\left|\Psi^{B1}_{2,-1}\right\rangle$	$\lambda_{2/3} = -3\sqrt{\frac{3}{2}}\xi_d \frac{V_{pd\pi}V_{pd\sigma}}{\delta\varepsilon_{pd}(\delta\varepsilon_{pd}+\tilde{\gamma}_1)}$
$\left|\Psi_{\Gamma_{E_{1,2}}}\right\rangle = \left|\Psi^{B2}_{1,0}\right\rangle - \frac{3}{\sqrt{2}}\frac{V_{pd\pi}}{\delta\varepsilon_{pd}}\left|\Psi^{A2}_{2,1}\right\rangle$	$\lambda^z_{3/3} = -\frac{9}{2}\xi_d \frac{(V_{pd\pi})^2}{\delta\varepsilon^2_{pd}}$

substrate have a different on-site energy Δ than atoms A2, B2 in the second layer. The most important terms are found to be

$$\hat{H}_{el}^{\text{eff}} = \hat{H}_{\text{chir}} + \hat{H}_{3w} + \hat{H}_{v_4} + \hat{H}_{\Delta},$$

$$\hat{H}_{\text{chir}} = -\frac{v_0^2}{\gamma_1}\begin{pmatrix} 0 & (\pi^\dagger)^2 \\ \pi^2 & 0 \end{pmatrix}, \quad \hat{H}_{3w} = v_3 \begin{pmatrix} 0 & \pi \\ \pi^\dagger & 0 \end{pmatrix},$$

$$\hat{H}_{v_4} = -\frac{2v_0 v_4}{\gamma_1}\begin{pmatrix} \pi^\dagger \pi & 0 \\ 0 & \pi \pi^\dagger \end{pmatrix},$$

$$\hat{H}_{\Delta} = \Delta \left[1 - \frac{v_0^2}{2\gamma_1^2}\pi^\dagger \pi \right]\begin{pmatrix} 1 & 0 \\ 0 & 0 \end{pmatrix}. \tag{B2}$$

*andor.kormanyos@uni-konstanz.de

[1] A. H. Castro Neto, F. Guinea, N. M. R. Peres, K. S. Novoselov, and A. K. Geim, Rev. Mod. Phys. **81**, 109 (2009).

[2] F. Guinea, A. H. Castro Neto, and N. M. R. Peres, Phys. Rev. B **73**, 245426 (2006).

[3] S. Latil and L. Henrard, Phys. Rev. Lett. **97**, 036803 (2006).

[4] C. L. Lu, C. P. Chang, Y. C. Huang, R. B. Chen, and M. L. Lin, Phys. Rev. B **73**, 144427 (2006).

[5] M. Aoki and H. Amawashi, Solid State Commun. **142**, 123 (2007).

[6] B. Partoens and F. M. Peeters, Phys. Rev. B **75**, 193402 (2007).

[7] A. Grüneis, C. Attaccalite, L. Wirtz, H. Shiozawa, R. Saito, T. Pichler, and A. Rubio, Phys. Rev. B **78**, 205425 (2008).

[8] M. Koshino and E. McCann, Phys. Rev. B **80**, 165409 (2009).

[9] M. Koshino and E. McCann, Phys. Rev. B **79**, 125443 (2009).

[10] M. Koshino, Phys. Rev. B **81**, 125304 (2010).

[11] F. Zhang, B. Sahu, H. Min, and A. H. MacDonald, Phys. Rev. B **82**, 035409 (2010).

[12] K. F. Mak, J. Shan, and T. F. Heinz, Phys. Rev. Lett. **104**, 176404 (2010).

[13] Ch. H. Lui, Zh. Li, Zh. Chen, P. V. Klimov, L. E. Brus, and T. F. Heinz, Nano Lett. **11**, 164 (2011).

[14] Ch. H. Lui, Zh. Li, K. F. Mak, E. Cappelluti, and T. F. Heinz, Nat. Phys. **7**, 944 (2011).

[15] W. Bao, L. Jing, J. Velasco Jr., Y. Lee, G. Liu, D. Tran, B. Standley, M. Ayko, S. B. Cronin, D. Smirnov, M. Koshino, E. McCann, M. Bockrath, and C. N. Lau, Nat. Phys. **7**, 948 (2011).

[16] L. Zhang, Y. Zhang, J. Camacho, M. Khodas, and I. Zaliznyak, Nat. Phys. **7**, 953 (2011).

[17] Th. Taychatanapat, K. Watanabe, T. Taniguchi, and P. Jarillo-Herrero, Nat. Phys. **7**, 621 (2011).

[18] T. Khodkov, F. Withers, D. Ch. Hudson, M. F. Craciun, and S. Russo, Appl. Phys. Lett. **100**, 013114 (2012).

[19] A. A. Avetisyan, B. Partoens, and F. M. Peeters, Phys. Rev. B **81**, 115432 (2010).

[20] R. Xiao, F. Tasnádi, K. Koepernik, J. W. F. Venderbos, M. Richter, and M. Taut, Phys. Rev. B **84**, 165404 (2011).

[21] F. Zhang, J. Jung, G. A. Fiete, Q. Niu, and A. H. MacDonald, Phys. Rev. Lett. **106**, 156801 (2011).

[22] F. Zhang, D. Tilahun, and A. H. MacDonald, Phys. Rev. B **85**, 165139 (2012).

[23] Y. Barlas, R. Cote, and M. Rondeau, Phys. Rev. Lett. **109**, 126804 (2012).

[24] V. Cvetković and O. Vafek, arXiv:1210.4923.

[25] J. Güttinger, C. Stampfer, F. Molitor, D. Graf, T. Ihn, and K. Ensslin, New J. Phys. **10**, 125029 (2008).

[26] M. F. Craciun, S. Russo, M. Yamamoto, J. B. Oostinga, A. F. Morpurgo, and S. Tarucha, Nat. Nanotechnol. **4**, 383 (2009).

[27] A. Kumar, W. Escoffier, J. M. Poumirol, C. Faugeras, D. P. Arovas, M. M. Fogler, F. Guinea, S. Roche, M. Goiran, and B. Raquet, Phys. Rev. Lett. **107**, 126806 (2011).

[28] E. V. Castro, M. P. López-Sancho, and M. A. H. Vozmediano, Solid State Commun. **152**, 1483 (2012).

[29] E. McCann and M. Koshino, Phys. Rev. B **81**, 241409(R) (2010).

[30] F. Guinea, New J. Phys. **12**, 083063 (2010).

[31] C. Ertler, S. Konschuh, M. Gmitra, and J. Fabian, Phys. Rev. B **80**, 041405(R) (2009).

[32] E. McCann and V. I. Fal'ko, Phys. Rev. Lett. **108**, 166606 (2012).

[33] H. Ochoa, A. H. Castro Neto, and F. Guinea, Phys. Rev. Lett. **108**, 206808 (2012).

[34] M. Diez and G. Burkard, Phys. Rev. B **85**, 195412 (2012).

[35] C. L. Kane and E. J. Mele, Phys. Rev. Lett. **95**, 226801 (2005).

[36] B. Dlubak, M.-B. Martin, C. Deranlot, B. Servet, S. Xavier, R. Mattana, M. Sprinkle, C. Berger, W. A. De Heer, F. Petroff, A. Anane, P. Seneor, and A. Fert, Nat. Phys. **8**, 557 (2012).

[37] M. Gmitra, S. Konschuh, Ch. Ertler, C. Ambrosch-Draxl, and J. Fabian, Phys. Rev. B **80**, 235431 (2009).

[38] S. Abdelouahed, A. Ernst, J. Henk, I. V. Maznichenko, and I. Mertig, Phys. Rev. B **82**, 125424 (2010).

[39] S. Konschuh, M. Gmitra, and J. Fabian, Phys. Rev. B **82**, 245412 (2010).

[40] S. Konschuh, M. Gmitra, D. Kochan, and J. Fabian, Phys. Rev. B **85**, 115423 (2012).

[41] J. C. Slater and G. F. Koster, Phys. Rev. **94**, 1498 (1954).

[42] G. Dresselhaus and M. S. Dresselhaus, Phys. Rev. **140**, A401 (1965).

[43] M. S. Dresselhaus, G. Dresselhaus, and A. Jorio, *Group Theory* (Springer-Verlag, Berlin, 2008).

[44] J. C. Boettger and S. B. Trickey, Phys. Rev. B **75**, 121402 (2007).

[45] S. Konschuh, Ph.D. thesis, University of Regensburg, 2011.

[46] R. Winkler, *Spin-Orbit Coupling Effects in Two-Dimensional Electron and Hole Systems* (Springer-Verlag, Berlin, 2003).

[47] S. Bravyi, D. DiVincenzo, and D. Loss, Ann. Phys. **326**, 2793 (2011).

[48] Zero matrix elements can arise, e.g., because we neglect remote direct hoppings between the first and the third layer except for the hopping A1-B3.

[49] The approximation $e^{-S} \approx 1 - S$ can be justified by the numerical calculations of Ref. 39. There it was shown that in the case of monolayer graphene $\frac{3}{2}\frac{V_{pd\pi}}{(\varepsilon_p - \varepsilon_d)} \approx 0.0871$. Since γ_2 is a small energy scale compared to $\delta\varepsilon_{pd} = \varepsilon_p - \varepsilon_d$, we find that $\tilde{V}_{pd\pi}/(\delta\varepsilon_{pd} - \gamma_2) \ll 1$. Furthermore, since $V_{pd\sigma}^{A1,B3}$ and $V_{dd\sigma}^{A1,B3}$ correspond to hopping between A1 and B3 atoms which are at larger distance than the A and B atoms within the same graphene layer, one can expect that $V_{pd\sigma}^{A1,B3} < V_{pd\pi}$ and $V_{dd\sigma}^{A1,B3} \propto \gamma_2$; hence both matrix elements of $S_{pd}^{(1)}$ in Eq. (4) are much smaller than unity.

[50] Ref. 30 considers an effective one-layer model and obtains a SOC Hamiltonian which is wave-number-independent and can be characterized by two SOC constants. One of the SO parameters, denoted by λ_1 in Ref. 30, corresponds to our $\lambda_{1/2}$. This can be seen by folding down the full Hamiltonian $\hat{H}_{ABC}$ to obtain a

low-energy effective model [see Eq. (12) in Sec. VI]. Further wave-number-independent SOC terms can also be obtained from the folding-down procedure, but they are higher order in the SOC parameters. Therefore we think that they are negligible with respect to the effective SOC Hamiltonian shown in Eq. (12). Ref. [45] explains the numerically calculated band structure with a single, diagonal SOC parameter.

[51] A. H. Castro Neto and F. Guinea, Phys. Rev. Lett. **103**, 026804 (2009).

[52] J. Klinovaja, G. J. Ferreira, and D. Loss, Phys. Rev. B **86**, 235416 (2012).

[53] C. Weeks, Jun Hu, J. Alicea, M. Franz, and Ruqian Wu, Phys. Rev. X **1**, 021001 (2011).

[54] O. Shevtsov, P. Carmier, C. Groth, X. Waintal, and D. Carpentier, Phys. Rev. B **85**, 245441 (2012).

[55] H. Jiang, Zh. Qiao, H. Liu, J. Shi, and Q. Niu, Phys. Rev. Lett. **109**, 116803 (2012).

[56] K.-H. Jin and S.-H. Jhi, arXiv:1206.3608.

[57] D. Marchenko, A. Varykhalov, M. R. Scholz, G. Bihlmayer, E. I. Rashba, A. Rybkin, A. M. Shikin, and O. Rader, Nature Commun. **3**, 1232 (2012).

[58] E. I. Rashba, Phys. Rev. B **79**, 161409 (2009).

[59] In general, if the inversion symmetry is broken there are ten SOC parameters in bilayer graphene. As in Ref. 40, we keep only the most important ones.

[60] E. Prada, P. San-Jose, L. Brey, and H. A. Fertig, Solid State Commun. **151**, 1075 (2011).

[61] F. Mireles and J. Schliemann, New J. Phys. **14**, 093026 (2012).

[62] More precisely, as we have already mentioned in connection with the intrinsic SOC (Ref. 50), when one folds down the full Hamiltonian one can obtain additional momentum-independent terms for the low-energy Hamiltonian but they are proportional to products and higher powers of the SOC parameters. We neglect these terms.

[63] E. McCann and M. Koshino, arXiv:1205.6953.